Low-velocity impact behavior of vitreous enameled steel plates

Andrea Zucchelli, Giangiacomo Minak, Daniele Ghelli

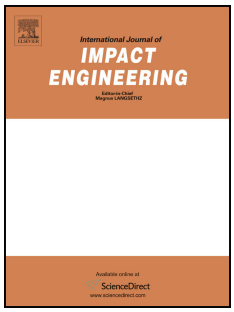

Title: Low-velocity impact behavior of vitreous enameled steel plates

Authors: Andrea Zucchelli, Giangiacomo Minak, Daniele Ghelli

PII: S0734-743X(09)00226-7

DOI: 10.1016/j.ijimpeng.2009.12.003

Reference: IE 1862

To appear in: *International Journal of Impact Engineering*

Received Date: 1 December 2008

Revised Date: 2 December 2009

Accepted Date: 10 December 2009

Please cite this article as: Zucchelli A, Minak G, Ghelli D. Low-velocity impact behavior of vitreous enameled steel plates, International Journal of Impact Engineering (2009), doi: 10.1016/j.ijimpeng.2009.12.003

Low-velocity impact behavior of vitreous enameled steel plates

Andrea Zucchelli, Giangiacomo Minak, Daniele Ghelli

University of Bologna, Mechanical Engineering Department

Viale Risorgimento 2, 40136 Bologna, Italy,

E-mail: a.zucchelli@unibo.it, giangiacomo.minak@unibo.it, daniele.ghelli@unibo.it

Key words: low velocity impact, vitreous enamel coating, instability, finite element analysis, residual stresses

ABSTRACT

In the present work vitreous enamel, a special class of ceramic-glass material, was used as a coating for thin steel plate. The impact behavior of rectangular steel plate and coated steel plate (enameled steel plate) was studied by means of both experimental tests and numerical analysis. Experimental tests revealed the onset and growth of plate instability in the case of impact both on steel plates and on enameled steel plates. The instability was mainly located on the free edges and was particularly evident on the longer side of rectangular plates. The impactor initial energy that caused the instability onset in the case of enameled steel plate was about six times higher than the one that induced the instability in the steel plates. Numerical simulations were performed to better understand and study the experimentally observed instability phenomenon. Four numerical models were developed in order to study the influence of plate thickness and residual stresses acting on the enameled steel plates on plate instability. Results of numerical simulation revealed that residual stresses acting on enameled steel plated increased the value of force that caused the instability onset. Further numerical simulations showed that the increase of residual stresses acting on enameled steel plates highlighted the values relative to the instability force increase according to a non linear trend.

1. Introduction

The vitreous-ceramic coatings used in this work belong to the class of enamels for metallic substrates known as porcelain- or vitreous-enamel coatings. Although these coatings are the oldest among known coatings for metals (the first examples appeared around 3000 years ago), we still know very little about their mechanical and tribological behavior. A wide spectrum of industrial and domestic applications currently make use of these coatings (e.g. the treatment of components for household use, the protection of interior walls of reactors for chemical processes, the protection of mechanical components of aircraft turbojets). Vitreous-enameled metals are non-equilibrium composites, since the enamel (a ceramic-glass material characterized by a predominantly amorphous structure whose percentage typically ranges between 85% to 95%, [1]) never exactly matches the metal (steel) over a range of temperatures. Since glass is a brittle material, and it almost always fails in tension, enamels are designed to be in a state of compression with respect to the metal on which they are applied [1,2]. This is accomplished by compounding the enamels so that they have a lower overall thermal contraction and expansion

than the metal, so that in cooling the enamel layer is placed under compression and the metal under tension. All enamel-metal composites, therefore, contain residual stresses which influence the overall physical and mechanical properties of the system.

Vitreous enamel coatings are also characterized by the presence of gas bubbles in the coating thickness (percentage of bubbles, known as blistering, typically range between 15% and 30%), and their surface is characterized by high values of hardness (up to 800 HV) and low roughness (lower than 0.5 μm). Compared to other coatings for metals, such as thermally sprayed ceramic ones, vitreous enamel coatings are characterized by a chemical and not only physical adhesion to the substrate achieved by a graded interface that is developed during the coating firing process. From the functional point of view, vitreous enamel coatings have an excellent resistance to chemical corrosion processes [1, 3-5] and a good resistance to tribological phenomena such as abrasive wear [4,5]. All these features can be totally lost or partially reduced by external phenomena, such as transversal loads, and in particular by low velocity impacts. In fact, such events can cause both the onset/growth of cracks and the spalling of the coating, thus decreasing the surface integrity and exposing the metal substrate to environmental attacks.

This paper discusses experimental tests of both steel and enameled steel plates that were subjected to low velocity impacts. Experimental results on both steel and enameled steel plates showed a structural instability when the initial kinetic energy of the impactor was greater than a certain threshold. It was also observed that in the case of enameled steel plates the instability onset energy was 6 times higher than in the case of steel plates. In both cases, steel plates and enameled steel plates, the instability took place, as a local instability, at the center of the longest edges and it was highlighted by a great change of specimen geometry, from the flat shape to the butterfly one, Figure 1.

A survey of the literature on this subject has shown a lack of experimental and theoretical studies about such instability. In fact the only paper that refers to the instability phenomenon considered here was published by Belluzzi in 1952 [6]. Experiments done by Belluzzi revealed the instability phenomenon in both rectangular and circular metal plates. Belluzzi related this instability phenomenon to a complex mechanism of load transfer within the plates. The author hypothesized that the transversal load leads to the development of compression membrane forces acting in the plane of the plate. The author also developed semi-empirical mathematical relations to predict the instability load, although he never completed the study. No references have been found about the impact behavior of enameled steel plates.

To reach a deeper understanding of the cited phenomenon, and to describe the mechanical behavior of both steel and enameled steel plates, numerical structural analyses were developed. Numerical simulations of steel plates confirmed the hypotheses by Belluzzi, even if in the case under study material nonlinear plastic behavior was observed. A good agreement between the maximum load measured during impact test on steel plates and the instability load from numerical analysis was observed. Also in the case of enameled steel plates, it was observed that the maximum load measured during impact test and the instability load from numerical analyses, that takes into account residual stresses, are in good agreement. By means of the numerical analyses it was also possible to highlight the influence of residual stresses acting on the enamel-metal composite on the instability load.

2. Materials and methods

2.1 Materials and experimental approach

Rectangular steel plates, 150mm x 100mm, made of very low carbon steel (DC04ED), were used as specimens for laboratory tests. One type of specimens were uncoated steel plates and a second type of specimens were very low carbon steel plates coated by vitreous enamel (also called enameled steel plates). The steel plate thickness was 0.8 mm while the average coating thickness was 200 μm per side. A special purpose enamel [5], technically used to protect the heating elements of rotary heat exchangers (ljungström type) in thermal power plants [7], was used as the material for coating. Enamel raw material was produced in water slip form by ball milling process [1]. Particulates of frits in the slip had a mean size of 0.40 μm ± 0.1μm. Enamel slip was applied over the steel specimen surfaces by wet-spray technology. Steel specimens covered by enamel slip were dehydrated and then fired at 870°C for 6 min 30 sec, obtaining a composite known as enameled steel. During the firing process the enamel raw material melts and interacts with the metal substrate, thus enabling the formation of a continuous varying structure. As shown in the micrograph of the transversal section in Figure 2, the interface zone between the substrate and the external layer is made of a complex material system where the vitreous enamel and the metal constituents are mixed. In particular, three main regions can be identified, starting from the bottom of Figure 2-A: a first region is made of metal, the second region is the interphase where both metal constituents and enamel components are mixed, and the third region composed of the vitreous enamel material. The presence of metallic dendrites that hinder the substrate and the external layer passing through the interphase region should also be noted, Figure2-B.

For the low velocity impact test on both enameled and not enameled plates, the same fixing support, designed according to ASTM [8], was used, Figure 3. A steel plate with a rectangular opening (125 mm by 75 mm) unilaterally supports the rectangular specimens. Three guiding pins ensure the correct positioning of tested plates so centering them with respect to the opening. Four levers with rubber tip prevent the upward motion of the plate during impact. The test apparatus was equipped with a laser sensor for measuring impactor velocity just before the collision.

The impactor was instrumented with a piezoelectric load cell to measure the contact force, and its overall mass was 1.22 kg. The impactor end-contact geometry was a hemisphere with a diameter of 12.7mm. The methodology adopted for the calculation of both impactor displacement and absorbed energy, at the impact stage, was also performed according to ASTM [8]. Low velocity impact tests were developed considering different energy levels (from 3J to 33J). The experimental protocol was articulated by first impacting the steel plates and then the enameled steel plates, see table 1 for the full test plan.

In order to perform numerical analyses the physical and mechanical properties summarized in table 2 for both low carbon steel and vitreous enamel coating materials were considered. In particular, the mechanical performance of low carbon steel was assessed by tensile tests according to UNI EN 10002. The mechanical properties of vitreous enamel material (E and ν) were estimated by four point bending and tensile tests [5]. The coefficient of thermal expansion of vitreous enamel material was determined by a heating dilatometer while the coefficient of thermal expansion for the metal was taken from the literature [1].

Figure 4-A shows the experimental stress-strain curve of the very low carbon steel plate tested in tensile condition. In the same figure, a six-point multilinear model used for the numerical simulations is also plotted. Figure 4-B shows an example of the load-displacement curve obtained

by tensile test of an enameled steel plate [5, 9, 10]. In particular, specimens for tensile tests were made from a low carbon steel sheet with 0.8 mm of thickness that was enameled on both sides with 0.2 mm thick enamel coating. In order to give a complete description of the diagram in figure 4-B, the residual stresses acting on the enameled steel specimens have to be taken into account.

In fact, as already mentioned in the introduction, the mechanical behavior of the vitreous enamel-metal composite at room temperature is greatly influenced by internal stresses developed during the enameling process. In the firing of an enamel, the sealing at elevated temperatures is accomplished without excessive stress development because the enamel is relatively fluid at the firing temperatures and can easily assume the surface dimensions of the metal to which it is applied. Any difference in the contraction of the metal and of the enamel is of little consequence until the temperature is reached at which the cooling rate is too rapid to allow flow of one on the other or internal flow in either. The stress developed initially is only a fraction of what would be expected when considering the difference in the rates of contraction of the metal and enamel. However, as cooling proceeds the amount of flow decreases and the rate of stress development becomes a function of differential contraction rates, moduli of elasticity, thickness, and shape. To reach a better understanding of this phenomenon, the expansion curves of both low carbon-steel and vitreous enamel have to be analyzed. Referring to Figure 5, it can be observed that although the metal has a straight-line thermal expansion relationship with temperature, the curve for enamel is not straight and undergoes a radical change in direction at about the Break Rate Temperature (BRT) [1], which is, in the case of the enamel used in the present study, about 400°C. Therefore, enamel has a lower expansion coefficient than low-carbon-steel when the temperature increases from the room temperature. The flow of the enamel substantially relieves the stresses during the heating and cooling of the composite at temperatures above the BRT. The amount of tension in low carbon steel and compression in enamel would actually be a function of the contraction differences in cooling from BRT to room temperatures during the cooling phase.

For a fixed component geometry, the intensity of residual stresses acting on the enameled steel composite can be pre-determined by means of the enamel design (compositions of frits and additions) aimed to match proper values of both BRT and coefficient of thermal expansion. In the present study only one type of enamel was studied, the same enamel used to manufacture the specimen used to determine the diagram in figure 4-B. On the basis of the knowledge of the coating thickness (0.2 mm per side) and of its coefficient of thermal expansion, it was possible to determine the maximum value of internal stress acting on the coating itself that was equal to 38 MPa [2,5]. Considering this value of internal stress and the load value at the first coating crack (4.1 kN) it was possible to determine the enamel coating strength equal to 35 MPa [2,5]. The value of enamel coating strength is used in the present work to perform the numerical simulations of enameled steel plates as the strength limit that can be reached by a coating element.

2.2 Numerical procedure

The numerical analysis were carried out considering a static loading process, because in these cases it was observed that the dynamic response of the specimens is dominated by the fundamental vibration mode and the contribution of higher ones was small.

In fact from experimental test it was observed that the force-displacement curves of both quasi-static and impact loading processes were mostly comparable (more details in § 3.2).

The numerical analyses were performed by ANSYS code, assuming a non-linear behavior with a multilinear law for the metallic substrate; on the contrary, for the enamel material a linear behavior, until its breakage, was assumed (table 2). To take into account the enamel coating failure, the element death procedure [11] was activated: if the maximum stress intensity of the coating elements exceeds the vitreous enamel strength its stiffness is reduced to zero. For both steel plate and enameled steel plate specimens the solution included the large displacement option. Moreover the pre-conditioned Conjugate Gradient iterative equation solver was used.

Due to the symmetry of the specimens, only one quarter of the plate was considered, figures 6 and 7. In order to avoid locking phenomenon and to reliably describe both the membrane and the bending behavior of the plate, the numerical model was made using SOLID186, a 20-node brick elements. The element technology was based on full integration (KEYOPT(2)=1) and the element formulation was based on pure displacement (KEYOPT(6)=0). In the thickness, one element was used for both steel and each enamel layer, and, as shown by the convergence test, the in-plane element average size was set to 1.5 mm. The contact area between the plate and the support was simulated by contact-pair elements implemented in ANSYS , assuming the standard type for the contact behavior and a coefficient of friction equal to 0.7 [12].

Constraint conditions respecting the full symmetry of the specimen quarter were applied in the x-y plane. Additional constraints in the z-direction, figure 7, were applied near the external part of specimens according to the fixing points in the experimental apparatus, figure 3. All the degrees of freedom of the support were fixed. Mechanical loadings were applied to nodes placed on the specimen surface at its inner corner (x=0, y=0), figure 7. The number of nodes to which forces were applied was four, thus allowing the simulation of the experimental contact area between the impactor and the specimen. The values of applied total force were greater than the maximum value of the contact force measured during impact tests at which the instability phenomenon took place. This choice was made in order to obtain information useful to estimate the force value that caused the plate instability onset. In the case of the enameled steel plates with residual stresses, a two load-steps solution process was chosen: the first load step was done to introduce the residual stresses related to the thermal manufacturing process of specimens, the second load step takes into account the mechanical loading. In particular for the first load step, according to the BRT previously mentioned, a temperature decrease of 400°C was applied to the full model. The two load steps approach was performed by the restart procedure included in the software [11].

The complete numerical analysis plan consisted in the following four numerical models:

1. simulation of a steel plate with a thickness of 0.8 mm (SIM-1)
2. simulation of a steel plate with a thickness of 1.2 mm (SIM-2);
3. simulation of an enameled steel plate, where the steel plate have a thickness of 0.8 mm and the thickness of the coating is 0.2 mm for each side of the specimen (thus achieving a total thickness of 1.2 mm); for this configuration two separate analyses were considered:
    - 3.a. simulation of an enameled steel plate where internal stresses are not taken into account (SIM-3); so in this case the solution was obtained by means of a single load step;
    - 3.b. simulation of an enameled steel plate where internal stress are taken into account (SIM-4); in this case a two load-step calculation was performed.

The first simulation, SIM-1, was used to study the experimental impact tests of the steel plates from the numerical point of view. The aims of this analysis were to compare the instability load calculated by numerical simulation to the one estimated by experimental test and to investigate the condition that caused the plate instability onset. The second, the third and the fourth simulations were aimed at evaluating the influence respectively of the plate material composition and of the internal stresses on the instability load. In fact, the last three simulations are characterized by the same specimens thickness, 1.2 mm, even if they differ because of both specimen material composition and internal stress state: in SIM-2 a steel specimen was analyzed, in SIM-3 and in SIM-4 a layered bi-material was considered but it must be noted that SIM-4 differs from SIM-3 because of the presence of internal stresses. In addition to the four described analyses, other simulations were performed to investigate the influence of residual stresses in enameled steel plates on the instability load. This study was developed considering the model of the enameled plate of SIM-4 but changing the coefficient of thermal expansion according to the following values: [1.00, 1.05, 1.10, 1.15, 1.20, 1.25] x 10^{-5} °C^{-1}. It should be also noted that the case of a 1.3x10^{-1} °C^{-1} coincides with SIM-3.

3. Results and Discussion

Results of the experimental tests and numerical analyses are respectively presented in the following two paragraphs.

3.1 Experimental test results and discussion

Figure 8 gives four examples of the post impact shape of both steel and enameled steel specimens. The diagrams in Figure 8 were obtained by laser scanning of the impacted surfaces. As previously mentioned, tests carried out on both steel plates and enameled steel plates highlighted the growth of a localized instability near the free edges of the plate. From these diagrams it can be observed that only when an energy threshold is overdrawn does instability takes place: in the case of steel plates the instability is caused by the impacts which have an energy between 3J and 6J, while in the case of enameled steel plates the instability energy threshold is between 24J and 33J.

Finally, according to post-impact geometries, we noted that the impact process led to a plastic behavior of the material.

In the case of enameled plates the impactor drop height that caused the growth of instability, and consequently the instability energy threshold, Figures 8 and 9, was higher than in the case of steel plates. Particularly by analyzing the photographs in Figure 9, it is possible to observe how in all cases the vitreous ceramic coating underwent significant damage in the central zone, with coating cracks and detachments, nonetheless, remaining basically adherent in those parts where the steel plate did not show instabilities. It is, thus, possible to observe that in the cases of E = 12 J, E = 18 J and E = 24 J, apart from the central zone surrounding the impact point, cracks in the coating do not seem to have caused spalling. Only a higher level of impact energy provoked a loss of coating in the areas where the instability appeared. Moreover, by comparing the images with E = 18 J and E = 24 J to E = 33 J it is possible to observe that the former already showed cracks which prelude a breaking of the enamel coating in the directions in which the last image shows the onset and growth of the instability.

Tests concerning impacts yielded useful information about the mechanical response of both steel and enameled steel plates in terms of force trend in the time domain and in terms of load versus impactor displacement. Moreover, the absorbed energy during impact was considered as a parameter of interest.

In the diagrams of Figure 10 we can see examples obtained during impacts of steel plates. In particular, we can observe that in the case of H=0.25m it was not possible to detect any drop in the load, diagrams A and B, which on the other hand can be seen for greater impact heights.

From the diagram of figure 10-D it can be observed that when the impact energy increases, the maximum force registered during the impact shows an increasing trend towards a horizontal asymptotic value. Moreover the trend of the absorbed energy during the impact compared to the kinematic energy on collision differs only slightly from the limit of the maximum absorbable energy, by the line in Figure 10-D. The trend of the force as a function of the kinematic energy on collision, together with the other trends shown in diagrams A, B and C, reveals that, when the instability takes place, the material elastic limit is exceeded and that, by increasing the height of fall, the extension of the plastic area tends to increase significantly (this statement is particularly backed by the trend of the absorbed energy compared to the height of fall).

Diagrams in Figure 11 on the contrary refer to impact tests on enameled plates. From the diagrams relating to the trend of the force, respectively versus time and displacement, figure 11-A & 11-B, it is possible to observe that only in the case of an impact from the maximum height, H=3.00m, do we have a marked drop after the maximum value of the force. Such a drop reveals the onset of the instability which, as has already been observed, is accompanied by the loss of the coating in the area where the instability takes place. In that sense, for both steel and enameled steel plates, it is particularly interesting to make a direct comparison between the trends of the force and the trends of the absorbed energy when the instability occurred. This comparison is shown in Figure 12. In particular, considering the impact force and the absorbed energy diagrams in figures 12 A and C we can observe a great difference in terms of the scale of values between the steel plates and enameled steel plates. On the other hand, if we consider the double scale entry diagrams in figures 12 B and C, a consistent similitude can be noted between the force diagrams and between the absorbed energy diagrams respectively of steel plates and enameled steel plates.

In the diagram related to the impact force, figure 12 A, it is possible to note, in both steel plates and enameled steel plates, a sudden drop in the force after the maximum peak followed by a second peak, less intense than the first, followed by a progressive decrease in the force with a typical “bell trend”. The trend of absorbed energies, Figure 12-D, behaves in a similar way. It is worth noting that the physical process that is at the basis of the first peak and drop of the force can be linked to the material yielding whereas the second peak and drop, having a lower intensity than the first, can be caused by a material hardening and/or structure stiffening phenomenon associated with the local instability. As far as this phenomenon is concerned, further details are given in the description of the numerical analysis results.

Finally. in Figure 13 we see the comparison between the maximum force and the absorbed energy registered during the impact and referring to the initial kinetic energy of the impactor at the collision stage. Concerning the maximum force values, it is possible to observe that they are always higher in the case of enameled plates than steel plates. On the other hand, as regards the absorbed energy during impact it is possible to observe that this is greater in the case of steel plates than in enameled ones. The facts cited and summarized in Figure 11-A and 11-B can be explained by taking two aspects into consideration: the enameled steel plates are thicker than the steel plates, and the enameled steel plates are subjected to a residual stress state (compression stress acting on the coating and tensile stresses acting in the metal substrate). In fact both aspects, specimen thickness and residual stress state, influence the impact behavior of enameled steel plates, causing a reaction to impact with a stronger force while dissipating a minor quantity of the impactor initial energy.

3.2. Numerical analysis results and discussion.

There are four main reasons why the description of the instability which was observed during the tests is very complex: (i) the instability is related to a local instability, (ii) the instability is caused by a state of stress internal to the plate which is induced by the transversal load, (iii) the buckled zones are characterized by large displacements and, moreover, (iv) the specimen constraint condition can be mostly considered unilateral (such as a simply supported constraint). The coincidence of these four aspects together with the material behavior which, as in our case, was experimentally verified to be plastic, makes the analytical approach an open issue. Nonetheless,

according to the goals of the present study, a decision was taken for research into the phenomenon which should be as faithful as possible. As was said in §.2, the numerical models which were developed integrate the four cited aspects.

The numerical analysis performed on steel plates, under a quasi-static loading process, enabled us to study the instability onset and growth. The quasi-static loading process was considered adequate to simulate the impacts because when considering, for example, the steel plate case, and comparing the experimental impact test to a quasi static indentation test, the force-displacement curves are mostly comparable, see figure 14. The reported quasi-static test was taken from the work [13] of the authors, where the instability of rectangular steel and enameled steel plates was investigated under a quasi-static indentation process. The quasi-static indentation process was done applying the load with the indenter also used in the present study with a head speed of 0.1 mm/sec.

In figure 14 it is possible to observe that, apart the initial stage of the test, where, in the case of the impact test the dynamic effect influences the contact force trend, the quasi-static trend of the force-displacement curve fits the impact curves well (to simplify the graph in the figure only the impact curve relative to the case where instability takes place, E =33 J, is reported).

Two images concerning the results of the simulation of the steel plate with a thickness of 0.8mm are shown in Figure 15. The two images refer to results obtained at an intermediate solution step (the percentage of the solution process is less than 80%) and at the end of the numerical simulation (100% of the solution process).

The image in Figure 15-A-1 and the associated diagram, Figure 15-A-2, respectively contain the contour map of the displacement and the vertical displacement of the plate's apexes corresponding to the sub-step after which the instability takes place. On the other hand, the image and the diagram in Figure 15-B-1 & 15-B-2 respectively represent the contour map of the vertical displacement and the vertical displacements at the apexes of the plate, points 1 and 2, at the last sub-step of calculus. We can observe that the diagrams in Figure 15-B-2 highlight the presence of a sudden change in the trend of Uz-1 and Uz-2 indicating the onset of the instability of the plate.

In order to analyze the instability and to identify the load in correspondence of which the instability takes place, the adopted procedure is based on the membrane and on the bending stress diagram, Figure 16. The membrane and bending stress component at x direction were calculated in the edge element where the displacement Uz-1 had also been evaluated. It can be noted that during the loading process the stresses components are characterized by two stages: the first part of the numerical simulation is dominated by a membrane behavior of the plate, after the critical load (the instability force value in figure 16-B) the plate is characterized by a bending behavior. Due to this change the butterfly shaped instability can take place. The diagram of the displacement Uz_1 of the apex edge node 1 highlight two main trends: the slow increasing trend and the fast increasing trend respect the loading process. The two trends are separated by the instability force value. In particular at the instability force value it can be noted a smooth change of the Uz_1 trend respect to the load and after that it has that small increment of the load cause a great increment of the displacement at the free apex 1.

In Figure 17 we can see the diagrams related to the trends of membrane and of bending stress calculated at the free apex 1 and considering the stress component respecting the x direction, while Table 3 reports the values of the instability force (F_{cr}).

A first observation of the values of critical load obtained by means of numerical simulations concerns the results of SIM-1 and SIM-4 which correspond to the two experimental cases previously discussed. Experimental results on steel plates showed that the impactor initial energy that causes the plate instability is between 3J and 6J, and, at the same time, the maximum force related to the plate instability onset due to impact is within a 1275 N ÷ 1560 N range. From the numerical point of view, it is interesting to note that the instability force value calculated by numerical simulation in the case of SIM-1, 1470 N is within the experimental force instability range A similar analysis can be done for the case of enameled steel plates. In fact, the impactor energy that causes the enameled plate instability is between 24 J and 33 J, while the maximum force related to the enameled steel plate instability is within a 4409 N ÷ 4694 N range. The force numerical value related to the plate instability, in the case of SIM-4, is 4570 N, a value that is coherent with the experimental result. Such observations suggest that the numerical simulation gave reliable calculations about the force value that causes the instability onset and growth for both steel plate and enameled steel plates.

It is also possible to note that:

(i) by increasing the thickness of the plate the critical load increases (see numerical results of SIM-1 and SIM-2),

(ii) The instability force in the case of enameled plates without considering residual stresses is higher than the case of steel plates with a thickness of 0.8mm (see comparison between SIM1 and SIM3), while it is lower if compared to the case of a steel plate with 1.2mm thickness (see comparison between SIM-2 and SIM-3),

(iii) The presence of a residual stress state tends to increase the value of the instability force compared to the case of a plate with an equivalent thickness, 1.2mm, but made of steel (see comparison between SIM-2 and SIM-4).

From these observations we can note the importance of the presence of residual stresses acting on the enameled plates on the critical load triggering the instability. This aspect was subjected to a further numerical research considering different values in the coefficient of thermal expansion of vitreous enamels to induce different states of residual stresses on the enameled plates. According to the values of the coefficient of thermal expansion cited in the material and method section, six simulations were carried out. The diagram (Figure 18) shows the results relating to these numerical analyses and the result of SIM-3 previously obtained.

From the diagrams it is possible to observe that with the increase of the value of the coefficient of thermal expansion there is a decrease of the residual stresses acting on the enameled plate (the coating tends to behave in the same way as the substrate from the point of view of thermal dilation) and in the same way the values relative to the instability force decrease accordingly.

4. Conclusions

The experimental study of the behavior to low velocity impact of steel plates and enameled steel plates, 0.8mm thick, allowed us to pinpoint the onset of a permanent local instability in the plates. The instability was marked on the longer side of the rectangular specimens and was considerable only when the impact exceeds a critical energy threshold. The experimental results

allowed us to detect that the critical energy for enameled plates is about 6 times that of non-coated plates. The numerical analyses of such a phenomenon were carried out considering the application of a quasi-static load using four reference models: steel plate 0.8mm thick, steel plate 1.2mm thick, enameled plate (with a substrate 0.8mm thick and a coating 0.2mm thick per each side) where residual stresses act and a porcelain plate where residual tensions do not act. For all models the material of the plate was described by means of a multilinear model, whereas for the enamel a brittle behavior was assumed integrated to the logic of the loss of stiffness for the elements that exceed material strength. The results of simulations pinpointed the onset of the instability at values that were very close to those obtained by means of experimental tests. Moreover, the results of the simulations, in their turn, pinpointed the importance of the residual stresses on the value of the critical load which caused the onset of the instability. In particular, it was established that the residual stresses raise the value of the very critical load. Lastly, a study concerning the influence of the residual stresses on the critical load induced by vitreous enamel coatings which are elastically equal but different as far as the thermal dilation coefficient is concerned, was carried out. This study highlighted a non-linear decrease on the instability force coinciding with the increase of the coefficient of thermal expansion to the limit of its equality to that of steel.

ACKNOWLEDGEMENTS

We wish to thank SMALTIFLEX S.p.A. for the preparation of coated specimens. Lastly, our thanks to Ing. Gabriele Cucciolini for the execution of the laser survey of the impacted plates.

BIBLIOGRAPHY

[1] Andrews A. I. *Porcelain Enamel*. The Garrard Press, 1961.

[2] R. Ambu, A. Zucchelli, L. Rossetti, V. Dal Re, Residual Stresses evaluation in Functionally Graded Composite Vitreous Enameled Steel Sheets, ETDCM8- 8th Seminar on Experimental Techniques and Design in Composite Materials 3-6 October 2007 – Sant'Elmo Beach Hotel – Castiadas – Costa Rei – Sardinia (Italy)

[3] R. Poletti, A. Zucchelli, A. Chelli, *Experimental Investigation on Corrosion Resistance of Porcelain Enamal Composite Coating for Regenerative Air Heaters Parts*, Danubia Adria 2005

[4] A. Chelli, R. Poletti, L.Pignatti, A. Zucchelli, L. Rossetti, V. Dal Re, S. Curioni, D. Prandstraller, S. Tiberi Vipraio, G. Palombarini, *Experimental study of the Mechanical and Tribological Properties of enameled steel plate (Studio delle Proprietà Meccaniche e Tribologiche di Lamiere in Acciaio rivestite mediante Smalti Porcellanati),* Smalto Porcellanato, CISP, 2006 (abstract in English, full text in Italian)

[5] A. Chelli, R. Poletti, L. Pignatti, F. Bruscoli, G. Pasqualetti, F. Bruni, A. Zucchelli, L. Rossetti, F. Lotti, G. Minak, V. Dal Re, S. Curioni, *Composite enameled steel elements for air preheaters and gas-gas heaters: an integrated approach from sheet forming and enamelling to basket assembly*, XXI° International Congress on Porcelain Enamel, pp. 130-158, 18-22 maggio 2008, Shanghai-China

[6] O. Belluzzi, A singular instability of thin plates that are supported at edges (Una singolare instabilità delle lastre sottili appoggiate al contorno), Giornale del Genio Civile, 1955, fasc. 1 (full text in Italian)

[7] ANSALDO, *Enamel coating for heating elements*, internal report, 1987.

[8] ASTM D 7136/D 7136M, *Standard Test Method for Measuring the Damage Resistance of a Fiber-Reinforced Polymer Matrix Composite to a Drop-Weight Impact Event*, November 2007.

[9] M.T. Kim, S.Y. Chang, O.Y. Oh, J.B. Won, H.W. Park, *Failure analysis of enamel-coated carbon steel heating elements of gas-gas heater for flue gas desulfurization system*, Engineering Failure Analysis 14 (2007) 686–693

[10] L. Rossetti, A. Zucchelli, V. Dal Re, *Caratterizzazione a Flessione e a Trazione di Rivestimenti Ceramico-Vetrosi applicati a Substrati Metallici (Bending and tension behaviour of enamled steel plates)*, XXXVI Convegno Nazionale AIAS – 4-8 Settembre 2007 Università degli Studi di Napoli Federico II – Seconda Università degli Studi di Napoli (abstract in english, text in italain)

[11] ANSYS user's manual, version v.11.

[12] ASM Handbook, Volume 18, Friction, Lubrication, and Wear Technology, 1992.

[13] A. Zucchelli, G. Minak. D. Ghelli, A Particular Instability of Unilaterally Supported Thin Plates Under Transversal Load: Effect of the Residual Stresses Induced by Vitreous Enameling, article in press, Blackwell Publishing Ltd j Strain (2009) doi: 10.1111/j.1475-1305.2009.00675.x

FIGURE CAPTIONS

Figure 1: examples of post-instability shape of a steel plate specimen

Figure 2: enamel-steel composite structure; (A) general micrograph view of the enamel and metal composite; (B) detail of the interface between the enamel coating and the metal substrate.

Figure 3: fixing apparatus for impact with impacted specimen

Figure 4: tensile test curves relative to (A) very low carbon steel and (B) enameled steel plates

Figure 5: thermal expansion diagram of the low carbon steel and of the vitreous enamel material used in the present study

Figure 6: numerical model of one quarter of the steel plate and enameled steel plate with details of the contact zone between plate and test device support

Figure 7: boundary conditions applied to the quarter model of the plate

Figure 8: images of impacted of steel plates and enameled steel plates obtained by laser scanning

Figure 9: photographs of 4 examples of porcelain plates having undergone an impact; in the case of an impact energy of E = 33 J the butterfly instability arises.

Figure 10: impact diagrams relating to steel plates; (A) time-force diagram, (B) diagram-displacement diagram, (C) time-absorbed energy diagram.

Figure 11: impact diagrams relating to enameled plates; (A) time – contact force diagram, (B) contact force – impactor displacement diagram, (C) time-absorbed energy diagram.

Figure 12: comparison between the contact force – time and absorbed energy – impactor displacement diagrams referring to tests where the instability was observed respectively in the case of steel plates and enameled steel plates.

Figure 13: comparison between the maximum force and the absorbed energy in the case of enameled and non-enameled plates for the different impact heights.

Figure 14: contact force and displacement in the case of the impact test (three energy comparisons at 33 J and in the case of quasi static indentation process

Figure 15: two images concerning the results of the simulation for a steel plate 0.8mm thick, corresponding to two solution sub-steps: (A) intermediate sub-step (77% of the overall solution process), (B) final sub-step (100% of the solution process).

Figure 16: (A) scheme for the stress data extraction from numerical results at position 1 and 3, (B) trend of bending and of membrane stresses respect to the x direction calculated on the basis of the stress respectively at 1 (Sx_1) and at 3 (Sx_3); (C) trend of the apex displacements, Uz_1.

Figure 17: trends of membrane (A) and of bending stress in x direction versus load.

Figure 18: trend of the critical load with the varying of the coefficient of thermal dilation of the coating and related trends of residual tensions in the substrate and the coating.

TABLES

Table 1: plan of impact test

Specimens type		Values					
Steel plate	Height [m]	0.25	0.50	1.00	1.50	2.00	\
	Energy [J]	3	6	12	18	24	\
Energy	Height [m]	\	0.50	1.00	1.50	2.00	2.75
	Energy [J]	\	6	12	18	24	33

Table 2: material properties

Material	α [10^{-5} °C^{-1}]	E [MPa]	ν
Low carbon steel (DC04ED)	1.30	180000	0.30
Vitreous enamel	1.08	70000	0.27

Table 3: values related to the instability force obtained by means of simulations for the four cases considered.

ID	Plate thickness [mm]	Enamel	Max residual stress [MPa]		F_{cr} [N]
			Steel plate	Enameled plate	
SIM-1	0.8	NO	\	\	1470
SIM-2	1.2	NO	\	\	2559
SIM-3	0.8	yes	0	0	2011
SIM-4	0.8	yes	41	-81.4	4570

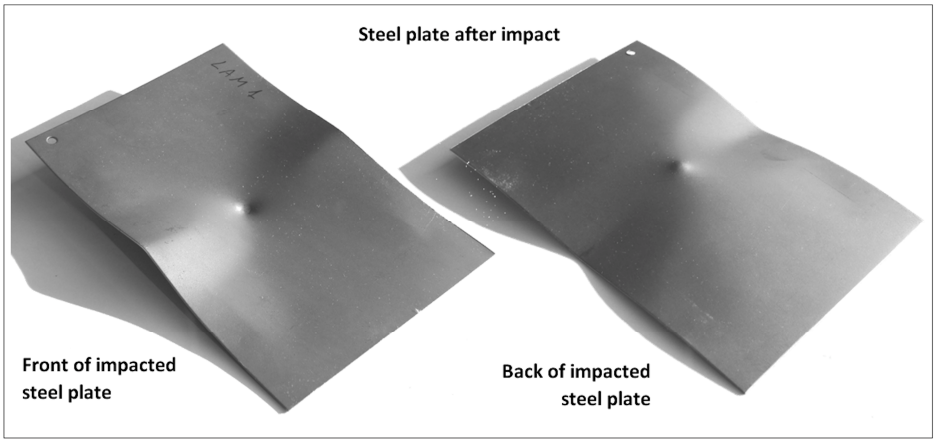

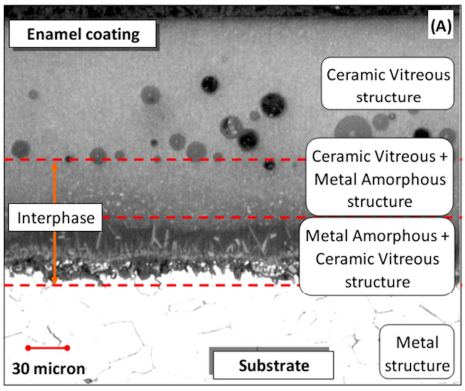

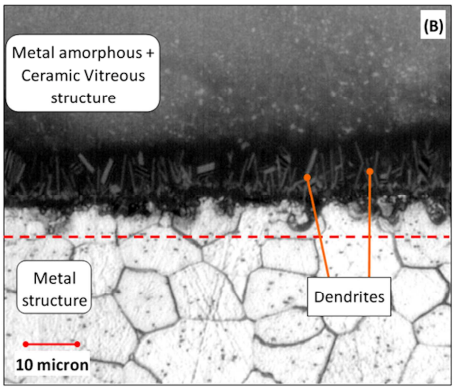

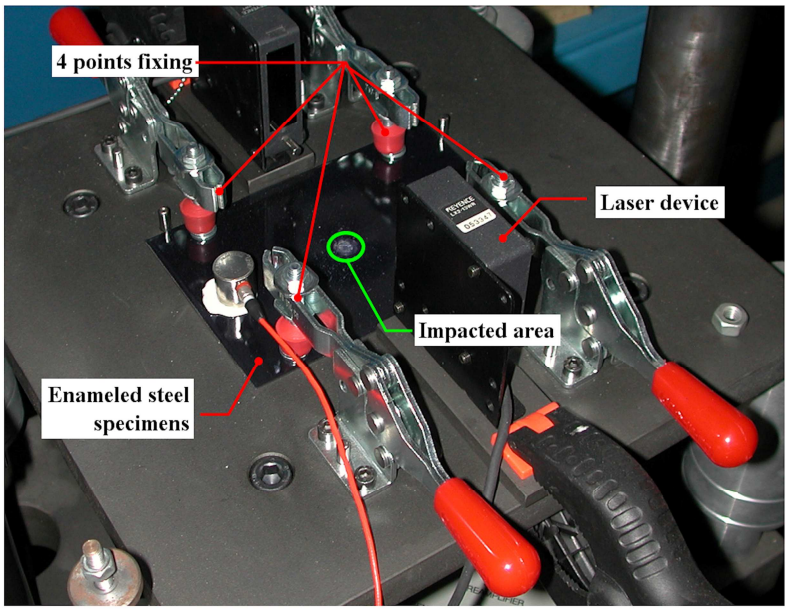

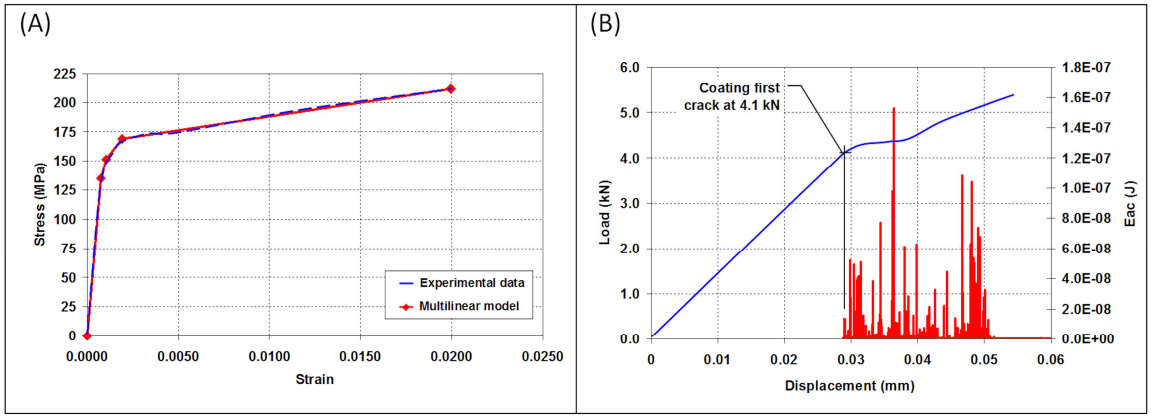

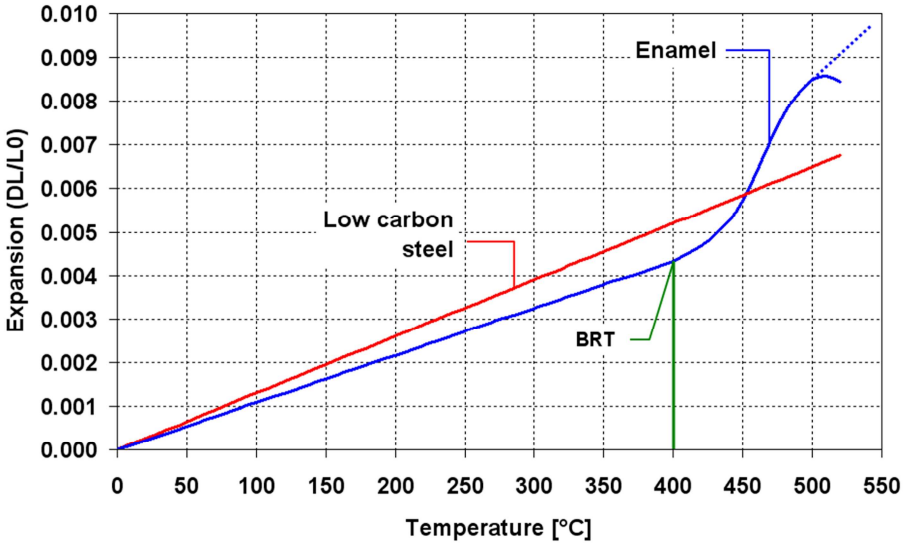

Numerical model of steel plate

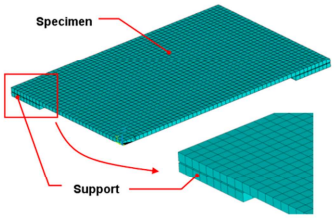

Detail of contact area

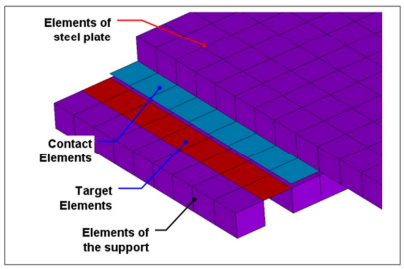

Numerical model of enameled steel plate

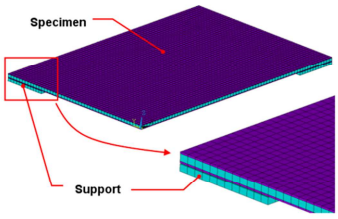

Detail of contact area